

The structure of ionization showers in air generated by electrons with 1 MeV energy or less

C Köhn¹ and U Ebert^{1,2}

¹ CWI, P O Box 94079, 1090GB Amsterdam, The Netherlands

² Eindhoven University of Technology, P O Box 513, 5600MB Eindhoven, The Netherlands

E-mail: koehn@cw.nl and ute.ebert@cw.nl

Received 20 January 2014, revised 28 March 2014

Accepted for publication 21 May 2014

Published 12 June 2014

Abstract

Ionization showers are created in the Earth's atmosphere by cosmic particles or by run-away electrons from pulsed discharges or by the decay of radioactive elements like radon and krypton. These showers provide pre-ionization that can play a role for discharge inception or evolution; radioactive admixtures in plasma technology use the same effect. While the CORSIKA program provides cross sections and models for cosmic particle showers down to the MeV level, we here analyze the shower structure below 1 MeV by using a three-dimensional relativistic Monte Carlo discharge code for the electron dynamics. We provide a few analytical results to speed up the numerical implementation of the scattering processes. We derive and analyze the spatio-temporal structure of ionization and electron energies in the shower for incident electrons with energies of 1 keV to 1 MeV, at air pressures of 10, 100 and 1000 mbar at room temperature in great detail. We calculate the final density of O_2^- and O^- ions and the average input energy per ion. We show that the average input energy per ion increases from 20 eV for initial energies of 1 KeV to 33 eV for 250 MeV. We also derive the electric fields generated by the electrons and residual ions of the particle showers. Finally, we study how the shower evolution and the electron energy at 1 bar is influenced by ambient electric fields of 5 or 8 kV cm⁻¹ and see that for 1 keV the electron number decreases, more slowly than without field, whereas the electron number continuously grows for 1 MeV.

Keywords: particle shower, ionization, attachment, low-energy, ambient electric field

(Some figures may appear in colour only in the online journal)

1. Introduction

1.1. Energetic particles and discharges

Energetic radiation in the atmosphere can contribute to discharge inception or it can influence discharge evolution. The primary motivation of our study are high-energy cosmic particle showers, but the results apply as well to ionization showers generated by radioactive decay [1] or by run-away electrons from powerful negative discharges like lightning leaders [2–5] or megavolt sparks [6, 7].

Cosmic particles with energies up to 10²⁰ eV [8] bombard our Earth and create extensive air showers. The detection and identification of the cosmic particles is of high current interest

for astroparticle physics [9–11], but their air showers also might play a role in lightning inception [12–14] or in triggering terrestrial gamma-ray flashes [15–17]. The high-energy part of these particle showers is well characterized by CORSIKA (COsmic Ray SIMulations for KAscade) which is a tool to simulate extensive air showers initiated by high-energy cosmic ray particles [18]. The initial incident particles can be protons, light nuclei up to iron ($Z = 26$), photons and electrons. CORSIKA simulates the particle showers they create in Earth's atmosphere, taking hadronic and electromagnetic interactions with air molecules into account [19, 20]. CORSIKA can also be used to calculate the production of neutrinos and Cherenkov radiation [21], i.e. radiation of electrons in dense media when they travel faster than the local speed of light. However, these

models do not resolve particle dynamics below 1 MeV which is the limiting energy for electron-positron pair production. On the other hand, common plasma discharge models and cross section data bases [22] extend only up to electron energies of 1 keV. Therefore there is a need to fill the gap and to derive the spatio-temporal distribution of electrons in the eV and the thermal range created by particles in the keV and GeV regime, in particular, when we want to study the sensitivity of these particle showers to ambient electric fields.

The same question arises when discharge inception is facilitated by radioactive admixtures. The streamer discharge experiments performed with an admixture of ^{85}Kr in [1] clearly show that the traces of the emitted β electrons with a maximal energy of 687 keV and an average energy of 251 keV have a different influence on discharge morphology than a more uniform background ionization.

1.2. Simulating showers created by electrons with energies ≤ 1 MeV

For particle energies of 1 MeV or below, the showers consist predominantly of electrons and positrons. Therefore we here simulate and characterize ionization showers created by electrons with initial energies between 1 keV and 1 MeV in air at room temperature for pressures of 10, 100 and 1000 mbar which correspond to altitudes in the atmosphere of 32, 16 and 0 km.

We use the Monte Carlo code in three spatial dimensions that was originally designed for streamer modeling and described in [23]; in simulations with this code run-away electrons with energies up to 3.5 keV were found [24]. We extended this code with relativistic equations of motion for the electrons and with cross sections for electron-nucleus bremsstrahlung, elastic scattering and ionization for electrons up to 1 MeV. We concentrate on electrons with initial energies of 1 MeV or lower as the high-energy models stop at this energy.

1.3. Content and organization of the paper

In section 2 we introduce the model. We discuss the collisions included, especially how we have implemented ionization, elastic, inelastic and reaction mechanisms. We also describe briefly how we include thermal effects. The results are presented in section 3. We plot and discuss the temporal evolution of the electron number and the spatio-temporal distribution of the electrons as well as the energy of the electrons and of the negative oxygen ions. We also calculate the electric field generated by the space charge separation within the particle shower. In section 4 we will show how an ambient field influences the shower. Section 5 summarizes our results and gives a brief outlook to future research. Details of our calculations regarding the ionization cross section which help to speed up calculations, can be found in appendix A and regarding the speed of oxygen ions in appendix B. In appendix C we briefly show how results change if we use different cross sections.

2. Cross sections and air temperature model

As the mass of air molecules is much higher than that of an electron, we consider them to be immobile and do not trace them. We implicitly place air molecules at random positions, thus as a constant background and draw random numbers to determine whether there is a collision of an electron with an air molecule and, if so, which collision takes place.

We model the motion of electrons in air which consists of 78.12% N_2 , 20.946% O_2 and 0.934% Ar. In most cases we do not consider any electric or magnetic field; hence there is no external energy source. Especially we do not take space charge effects into account; thus the physics of such showers do not depend on the initial electron number. For an initial electron energy of 1 keV and 1 MeV we will also include an ambient electric field. We include ionization [25], elastic scattering [22, 26–30], electron-nucleus bremsstrahlung [31, 32], excitations [22, 33] and attachment [33, 34]. We note here that we ran also simulations where we trace bremsstrahlung photons and included photoionization. However, we have not seen any significant changes to the results presented here.

2.1. Elastic scattering

Our particle code was originally developed to study streamer dynamics [23] where electrons reached energies up to 3.5 keV in the simulations of [24]. For electron energies below 10 keV, we use cross sections by [27–30] as distributed by LXcat [22]. For energies above 10 keV, we extended the energy range of the total cross section for elastic scattering with a screened Rutherford expression [26, 35]

$$\sigma(E_{\text{kin}}) = \frac{2\pi Z^2 e^4}{v^2 p^2 \eta(\eta + 1)}, \quad (1)$$

where v , p and η depend on E_{kin} as

$$v = \sqrt{c^2 - m_e^2 c^6 / (E_{\text{kin}} + m_e c^2)^2},$$

$$p = \sqrt{(E_{\text{kin}} + m_e c^2) / c^2 - m_e^2 c^2}$$

and

$$\eta(E_{\text{kin}}) = \frac{\chi_0^2}{2} \left[1 + 4\alpha Z \chi_0 \left(\frac{1 - \beta^2}{\beta} \ln \chi_0 + \frac{0.231}{\beta} + 1.448\beta \right) \right] \quad (2)$$

with $m_e \approx 9.1 \times 10^{-31}$ kg, $\beta(E_{\text{kin}}) = v/c$, $\alpha \approx 1/137$, $\chi_0(E_{\text{kin}}) = \hbar \mu Z^{1/3} / (0.885 p a_0)$, $e \approx 4.80 \times 10^{-10}$ esu and $a_0 \approx 2.82 \times 10^{-13}$ cm where E_{kin} is the kinetic energy of the electron and Z is the atomic number. $\hbar \approx 1.05$ J s is the reduced Planck constant, and $\mu = 0.635$ is a fitting parameter ensuring a continuous transition from (1) to experimental data of energies below 10 keV.

For the azimuthal angle we use [35, 36]

$$\frac{d\sigma}{d\Omega}(E_{\text{kin}}, \theta) = \frac{\sigma(E_{\text{kin}})}{4\pi} \cdot \frac{4\eta_1(1 + \eta_1)}{(1 - \cos \theta + 2\eta_1)^2} \quad (3)$$

with $\eta_1 = 5.77 \cdot E_{\text{kin}}^{-1.377}$. The polar angle φ is equally distributed over $[0, 2\pi)$.

2.2. Ionization cross section

To model ionization we use the relativistic binary-encounter Bethe (RBEB) total cross section $\sigma(E_{\text{kin}})$ and the differential cross section $d\sigma/dW(E_{\text{kin}}, W)$ [25] where E_{kin} and W are the energies of the incident and the ejected electron, respectively. W can be obtained by solving [37]

$$R = \frac{\int_{E_{\text{min}}}^W \frac{d\sigma}{d\bar{W}}(E_{\text{kin}}, \bar{W}) d\bar{W}}{\int_{E_{\text{min}}}^{\frac{E_{\text{kin}}}{2}} \frac{d\sigma}{d\bar{W}}(E_{\text{kin}}, \bar{W}) d\bar{W}} \quad (4)$$

where $R \in [0, 1)$ is a uniformly distributed random number, and $E_{\text{min}} = 0.01$ eV is the lower threshold for the energy of secondary electrons. We have derived an explicit expression (A.9) for the integrals in (4) that can be found in appendix A. We solve (A.9) by using the regula falsi method [38]. The scattering direction of the electron is parameterized by the angles $\Theta_{\text{sca}} = \angle(\mathbf{p}_i, \mathbf{p}_{\text{sca}})$ and φ_{sca} , and the direction of the emitted electron relative to the incident electron is $\Theta_e = \angle(\mathbf{p}_i, \mathbf{p}_e)$ and φ_e . Here \mathbf{p}_i is the momentum of the incident electron before scattering, \mathbf{p}_{sca} its momentum after scattering and \mathbf{p}_e the momentum of the emitted electron. $\Theta_{\text{sca},e}$ are given by [37]

$$\cos \Theta_{\text{sca}} = \sqrt{\frac{(E_{\text{kin}} - W)(E_{\text{kin}} + 2m_e c^2)}{E_{\text{kin}}(E_{\text{kin}} - W + 2m_e c^2)}} \quad (5)$$

$$\cos \Theta_e = \sqrt{\frac{W(E_{\text{kin}} + 2m_e c^2)}{E_{\text{kin}}(W + 2m_e c^2)}}. \quad (6)$$

The polar angles $\varphi_{\text{sca},e}$ are uniformly distributed on $[0, 2\pi)$.

2.3. Electron attachment

After having lost energy by collisions, electrons can attach to oxygen through two processes [33, 34, 39]: An electron can split an oxygen molecule (two-body or dissociative attachment)

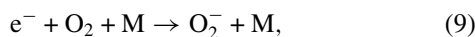


where the binding energy is $E_{\text{bind}} = 5.2$ eV. The speed of O^- and O is

$$v_{\text{O}} = v_{\text{O}^-} = \sqrt{\frac{m_e |v|^2}{2m_{\text{O}}} - \frac{E_{\text{bind}}}{m_{\text{O}}}}, \quad (8)$$

where v is the velocity of the incident electron and $m_{\text{O}} \approx 2.6568 \times 10^{-26}$ kg is the mass of an oxygen atom or ion. Details of the derivation of (8) can be found in appendix B.

An electron can also attach to an oxygen molecule directly, but only in the presence of a further molecule to conserve energy and momentum (three-body attachment)



where M is N_2 or O_2 [33, 34]. Since three-body attachment needs the presence of two molecules, the rate of this process depends on air density, not linearly, but quadratically.

2.4. Air temperature

Our first simulations have shown that the energy of electrons continues to decrease to below 0.025 eV. The lower threshold energies for two- and three-body attachment are 4.4 eV and 0.07 eV, respectively. Therefore at vanishing air temperature, there are always very low energy electrons that stay free. Therefore we have included the thermal energy of the neutral air molecules at 300 K (corresponding to 0.025 eV) for collisions with electrons with kinetic energies below 1 keV with the method described in [40]. Here the energy E_n of the neutral is sampled from the Maxwell–Boltzmann distribution

$$f(\epsilon) = \sqrt{2\epsilon} e^{-\epsilon + \frac{1}{2}} \quad (10)$$

with $\epsilon = E_n/(k_B T)$ and $k_B \approx 1.38 \times 10^{-23}$ J K⁻¹.

3. Results

3.1. Evolution of electron and ion number in the shower

We performed simulations for incident electrons with energies of 1, 10, and 100 keV and 1 MeV. In the first three cases we averaged our results over 100 initial electrons, while for 1 MeV there was already sufficient self-averaging with a single electron starting the shower. We studied the showers in air at 10, 100 and 1000 mbar at room temperature.

Figure 1 shows the electron number in the shower as a function of time. Within our simulations the electrons move only by some 100 μm to 30 cm (see section 3.3 for the shower length). Thus pressure variations within the simulation volume are negligible.

In all cases, first the electron number increases while the shower develops, then it reaches a plateau (except for 1 MeV where the plateau is less pronounced), and finally the electron number decreases due to attachment to oxygen. Starting with an electron with 1 keV at 1 bar, the maximal electron number within the shower is 37.4 ± 2.6 electrons; for 1 MeV, it is approximately 34 000. We determined the error in the electron number for 1 keV by running 20 simulations with one initial electron and different realizations of random numbers. For higher initial energies the statistics becomes better and thus the error becomes smaller. Table 1 shows the initial electron energy E_0 and the maximal electron number $N_{\text{max}}(E_0) = \max_t N_e(E_0, t)$; the average input energy $E_0/N_{\text{max}}(E_0)$ per electron ranges from 27.03 eV for $E_0 = 1$ keV up to 29.52 eV for $E_0 = 1$ MeV independently of pressure p . For comparison, the ionization energy of N_2 is 15.6 eV, and of O_2 12.06 eV.

As expected, the electron density essentially decreases due to electron attachment to oxygen though recombination is included. Figure 3(a) shows the production of O_2^- and O^- ions as a function of time for an incident electron with 1 keV energy. Note that the maximal number of oxygen ions is larger than the maximal electron number as some electrons continue to ionize more molecules while other electrons already attach. For all electron energies and for 1 bar as well as for 100 mbar the production of O_2^- ions is the dominant process, while the number of O^- increases for smaller pressure until two-body attachment and the subsequent formation of O^- is the dominant

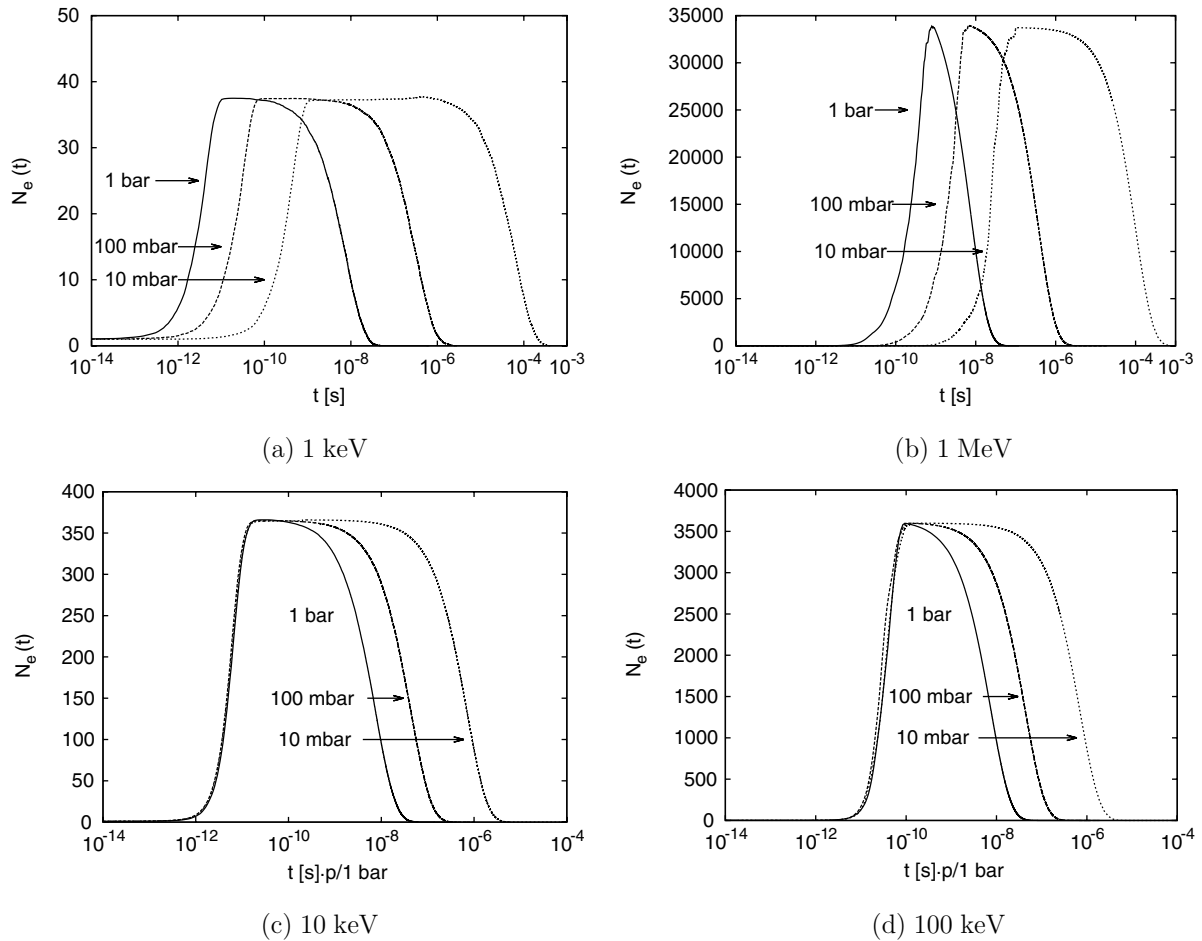


Figure 1. The electron number in a shower as a function of time generated by one initial electron with an energy E_0 of (a) 1 keV, (b) 1 MeV, (c) 10 keV and (d) 100 keV for 10, 100 and 1000 mbar. For 1, 10, and 100 keV we averaged over 100 runs. In (c) and (d) the plots for 100 mbar (10 mbar) were shifted by a factor 10 (100) on the time axis.

process at 10 mbar. Figure 3(b) shows the electron number and the added number of electrons and O_2^- ions and of electrons, O_2^- and O^- ions for 1 keV and 1 bar. It shows that when the electron number starts to decrease, first the number of O_2^- ions starts to increase; after approximately 10 ns there is also an effect of O^- ions. Table 1 shows that the ratio of the initial energy E_0 and the maximal number $N_{i,\max}(E_0) = \max_t N_i(t, E_0)$ of positive ions varies from 19.23 eV for 1 keV up to 21.17 eV for 1 MeV. Figure 2(a) shows the average input energy per ion as a function of the initial energy E_0 . It shows that the average input energy per ion increases with increasing E_0 . For $E_0 = 250$ MeV, $E_0/N_{i,\max}$ is approximately 33 eV which agrees well with 33.38 eV as given in [41]. Above that energy the average input energy saturates. Figure 2(b) shows the energy distribution of secondary electrons from impact ionization as a function of the energy W of the secondary electron. It shows that for all shown incident electron energies $E_{\text{kin},i}$ the maximum of the distribution lies at approximately 7 eV. For a given probability which is proportional to the differential cross section, electrons with small incident energies eject electrons with higher secondary energies than electrons with high incident energies. Thus, if secondary electrons have more energy, they can perform more ionizations and thus the average input energy per ion decreases. The plot in panel (b) also shows that the energy distributions for 100 MeV and 1 GeV are alike;

Table 1. The maximal electron number $N_{e,\max}$, the ratio $E_0/N_{e,\max}$, the maximal number $N_{i,\max}$ of positive ions and the ratio $E_0/N_{i,\max}$ as a function of the initial energy E_0 .

E_0	$N_{e,\max}(E_0)$	$E_0/N_{e,\max}(E_0)$	$N_{i,\max}(E_0)$	$E_0/N_{i,\max}(E_0)$
1 keV	37	27.03 eV	52	19.23 eV
10 keV	363	27.55 eV	514	19.46 eV
100 keV	3595	27.82 eV	5000	20.00 eV
1 MeV	33 875	29.52 eV	47 235	21.17 eV

thus the average input energy per ion saturates for energies above 100 MeV.

The probability $P(n)$ of exactly n subsequent ionizations by secondary electrons is proportional to $\int_{E_{n-1}}^{E_n} \frac{d\sigma}{dW}(E_{\text{kin},i}, W) dW / \int_{E_{n-1}}^{E_{\text{kin},i}/2} \frac{d\sigma}{dW}(E_{\text{kin},i}, W) dW$ where $[E_{n-1}, E_n]$ is the energy interval of a secondary electron to produce exactly n subsequent ions. We can estimate the energy of one more impact ionization: The ionization energy of N_2 which contributes 80% to air, is approximately 15.6 eV. The average excitation energy before ionization is approximately 4.2 eV [42]; thus if the energy of a secondary electrons is below 19.8 eV, there is no expected further ionization. If the energy is above 19.8 eV there is at least one more ionization. The most expected value of the tertiary electron is 9.1 eV [25];

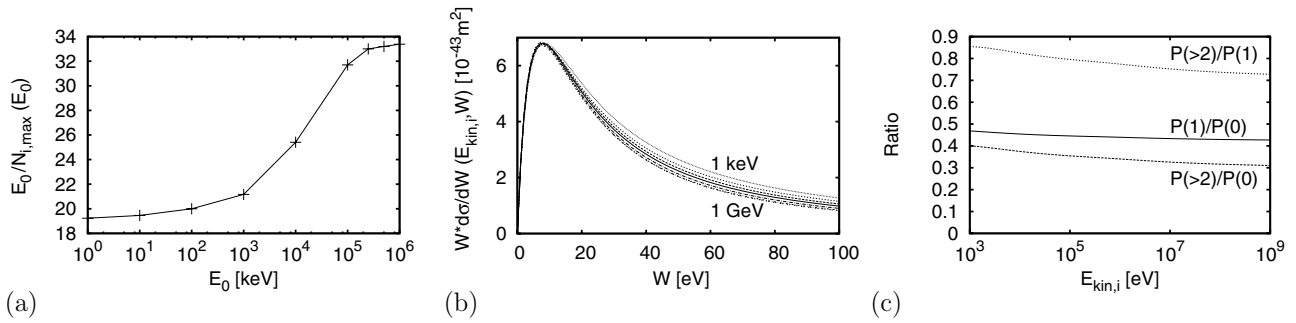


Figure 2. (a) The average input energy per ion as a function of the initial electron energy E_0 . (b) The energy distribution $W \cdot d\sigma/dW$ for ionization as a function of the secondary electron energy W . $d\sigma/dW$ is given by (A.4). All distributions are normalized to the same maximum. The different lines represent different incident energies $E_{\text{kin},i}$ of the primary electron between 1 keV and 1 GeV and increasing by factors of 10. (c) The ratio of the probabilities of subsequent ionizations by secondary electrons as function of incident electron energy $E_{\text{kin},i}$. $P(0)$ and $P(1)$ denote the probabilities of no more or only one more subsequent ionization; $P(> 2)$ denotes the probability of two or more subsequent ionizations.

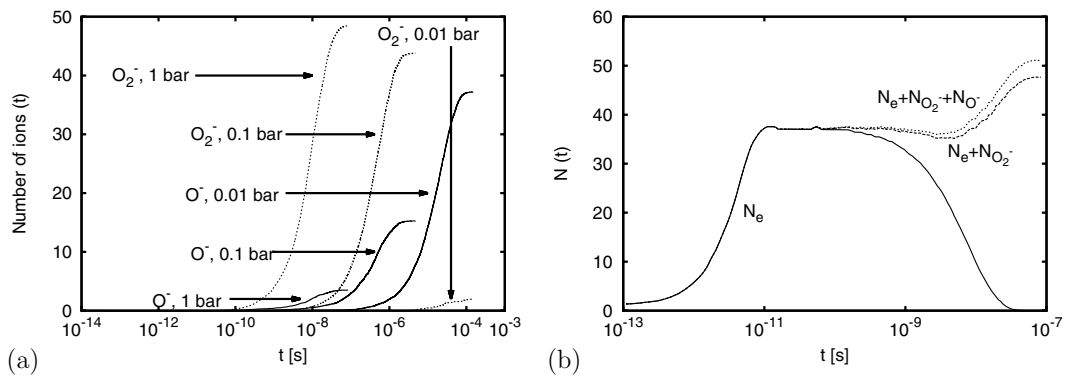


Figure 3. (a) The number of O_2^- (dotted line) and O^- (solid line) ions as a function of time for an air shower at 1000, 100 and 10 mbar generated by an electron of 1 keV energy. (b) The number of electrons (solid line), of electrons and O_2^- ions (dashed line) and of electron, O_2^- and O^- ions (dotted line) as a function of time for 1 keV and 1 bar. The dip at approximately 10 ns is due to recombination with positive ions.

if this electron has also 19.8 eV, hence in total 48.7 eV, it could produce 2 subsequent ions. Hence, if the energy of the secondary electron is between 19.8 eV and 48.7 eV, it will do exactly one more ionization. If it is above 48.7 eV it will do more than two subsequent ionizations. Figure 2(c) shows the ratios of probabilities of subsequent ionizations by secondary electrons as a function of the incident electron energy. It shows that more than one subsequent ionization is expected rather for small incident electron energies than for high incident energies. Thus more ions are expected for small initial energies and the ratio of $E_0/N_{i,\max}$ decreases.

3.2. Growth and decay rates

Figure 1 also shows the lifetime of the electron swarm. For 1 bar it takes 65 ns until all electrons have attached. For 100 mbar it takes approximately 2 μs and for 10 mbar it takes 0.5 ms. That is because electrons need time to lose enough energy through ionization, inelastic scattering and the production of bremsstrahlung photons to reach the energy range where attachment can occur.

Figure 4 explicitly shows how the electron number depends on the initial energy E_0 of the incident electron. The relative electron number per E_0 decreases a bit with increasing initial energy, but is equal for all electron energies after 10 ns. This is because for high initial electron energies,

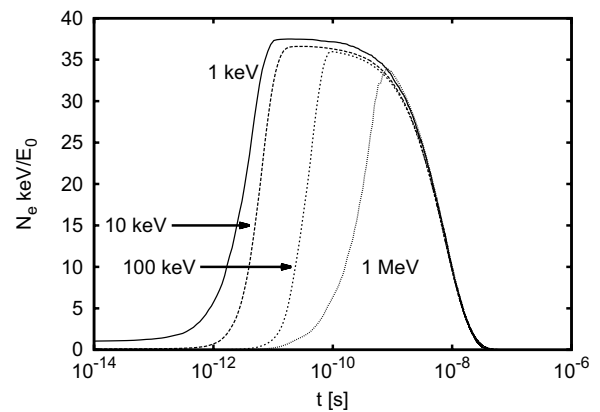


Figure 4. The electron number per initial energy $N_e \text{ keV}/E_0$ as a function of time for initial electron energies $E_0 = 1 \text{ keV}$, 10 keV, 100 keV and 1 MeV for 1 bar.

different subshowers develop at slightly different times and their maxima will not occur simultaneously. Hence the maximal electron number in a shower of a 1 keV electron is larger than 1/1000 times the maximal electron number in a shower of a 1 MeV electron.

3.2.1. Growth rate. Furthermore figure 1 shows that the temporal evolution of the electron number depends on pressure.

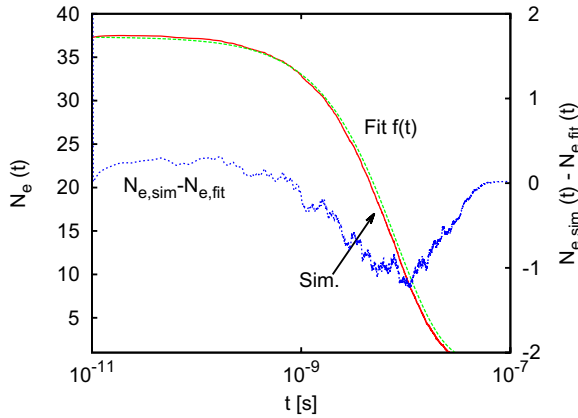


Figure 5. The electron number as a function of time for $E_0 = 1$ keV and 1 bar. ‘Sim.’ (red line) denotes the number calculated in our simulation and ‘Fit’ (green line) denotes Equation (12). The blue line denotes the difference of the simulation results and (12).

Panels (c) and (d) in the figure are explicitly constructed to show that the growth rate of the electron number depends on air density (and pressure) according to Townsend scaling

$$N_e(p/\delta, t \cdot \delta) = N_e(p, t), \quad (11)$$

where δ is an arbitrary number. Here $N_e(p, t)$ is the electron number as a function of pressure and time. This Townsend scaling is due to the fact that the shower growth is dominated by impact ionization which is a two-body process, whose rate scales with the gas density. Hence the intrinsic shower growth times (for a given electron energy) are inversely proportional to the gas density.

3.2.2. Decay rate. However, the electron shower does not decay due to a fixed scaling law. This is related to the fact that for higher pressures the three-body attachment dominates whose rate depends quadratically on the air density; while for lower pressures (below 100 mbar) the two-body process of dissociative attachment takes over, as discussed above.

Figure 5 shows an example of an exponential fit to the decay of the electron number for $E_0 = 1$ keV and 1 bar where

$$N_e(t) = N_{\max}(E_0) e^{-t/\tau(E_0, p)}. \quad (12)$$

The blue lines shows the difference of the electron number of the simulation and of the fit; the difference is at most 1 electron. This exponential fit is very good, mainly because the electrons approach a rather stationary energy distribution at this stage as we will show below, hence the energy dependent attachment rates do not vary in time. (This is also the reason why an exponential curve does not fit the shower growth well.)

Table 2 shows the values of $\tau(E_0, p)$ for the smallest and highest energies and pressures that we have investigated. Both the table and figure 4 show that the decay of the electron shower does not depend on the energy E_0 of the incident electron.

We finally remark that [1, 43, 44] state that an electron shower initiated by a 1 keV electron in air at standard temperature and pressure has an attachment time of approximately 10 ns, which agrees well with our simulation result of 8.19 ns.

Table 2. Parameters $N_{\max}(E_0)$ and τ to fit Equation (12) to the electron number as a function of time as in figure 5.

E_0	p	$N_{\max}(E_0)$	$\tau(E_0, p)$
1 keV	1 bar	37.34	8.19 ns
1 keV	10 mbar	37.34	61.02 μ s
1 MeV	1 bar	33 875	8.19 ns
1 MeV	10 mbar	33 875	1.97 μ s

3.3. Spatial structure of the shower

3.3.1. Shower at 1 keV and 1 bar. Figure 6 shows structure and evolution of the electron shower created by an electron with initial energy $E_0 = 1$ keV moving in z direction from the origin of the coordinate system. Until all electrons have attached, the furthest electron moved about 0.5 mm. The extension of the electron cloud at 1 ns is

$$(\Delta x, \Delta y, \Delta z) \approx (90 \mu\text{m}, 80 \mu\text{m}, 100 \mu\text{m}), \quad (13)$$

where Δx is defined as

$$\Delta x := |\max(x) - \min(x)|, \quad (14)$$

and $\max(x)$ ($\min(x)$) is the maximum (minimum) of all x coordinates of all electrons at a given time. Δy and Δz are defined in the same manner.

3.3.2. Shower at 1 MeV and 1 bar. For an incident electron energy of 1 MeV figure 7 shows the electron swarm at approximately 0.8 ns when the electron number is maximal. We here started with one (panel (a) and (b) for different realizations of random numbers) and 20 (panel (c)) electrons beamed in z direction. Panel (a) shows that the initial electron moves forward and leaves a trace of secondary electrons behind. Panel (b) shows the behavior of one single initial electron for different random numbers. It shows that the strictly forward motion in panel (a) is just one example; in panel (b) the initial electron moves a bit to the side leaving residual electrons behind. Panel (c) shows the position of all electrons projected onto the xz plane for 20 initial electrons. It shows the different trajectories of the high-energy initial electrons.

Figure 8 shows the time evolution of the electron number projected on the z axis for 20 initial electrons. It shows that the electron number per bin Δz increases in time and that the swarm moves in forward direction. It also shows that for 0.8 ns most electrons are located at $z < 12$ cm and only a few electrons lie beyond 12 cm.

3.4. Swarm induced electric field

Since the electrons move, leaving the positive ions behind, an electric field will be induced by the space charges. This field can be calculated from the positions \mathbf{r}_j of electrons and ions at different time steps as

$$\mathbf{E}(\mathbf{r}, t) = \frac{e}{4\pi\epsilon_0} \left(- \sum_{j=1}^{N_e(t)} \frac{\mathbf{r} - \mathbf{r}_j}{|\mathbf{r} - \mathbf{r}_j|^3} + \sum_{j=1}^{N_{i+}(t)} \frac{\mathbf{r} - \mathbf{r}_j}{|\mathbf{r} - \mathbf{r}_j|^3} - \sum_{j=1}^{N_{i-}(t)} \frac{\mathbf{r} - \mathbf{r}_j}{|\mathbf{r} - \mathbf{r}_j|^3} \right), \quad \mathbf{r} \neq \mathbf{r}_j, \quad (15)$$

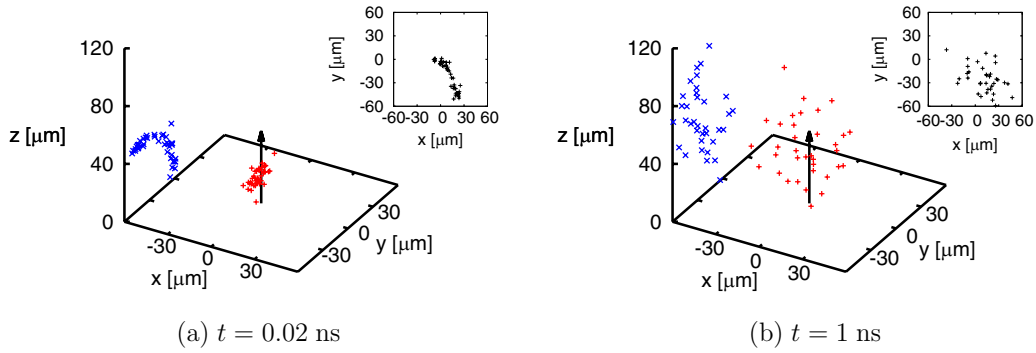


Figure 6. The evolution of an electron shower in air at 1 bar and 300 K with a particular realization of random numbers. The incident electron has an energy of 1 keV; its initial direction of motion is indicated by the arrow; this initial electron attaches at 0.5 ns. The electron number is maximal at 0.02 ns. The electron number reaches zero after approximately 20 ns. The electron positions are indicated by red crosses in three-dimensional space at times (a) 0.02 ns and (b) 1 ns. The blue points indicate the projection of the electrons onto the xy plane. The insets show the position of the electrons projected onto the xy ground plane.

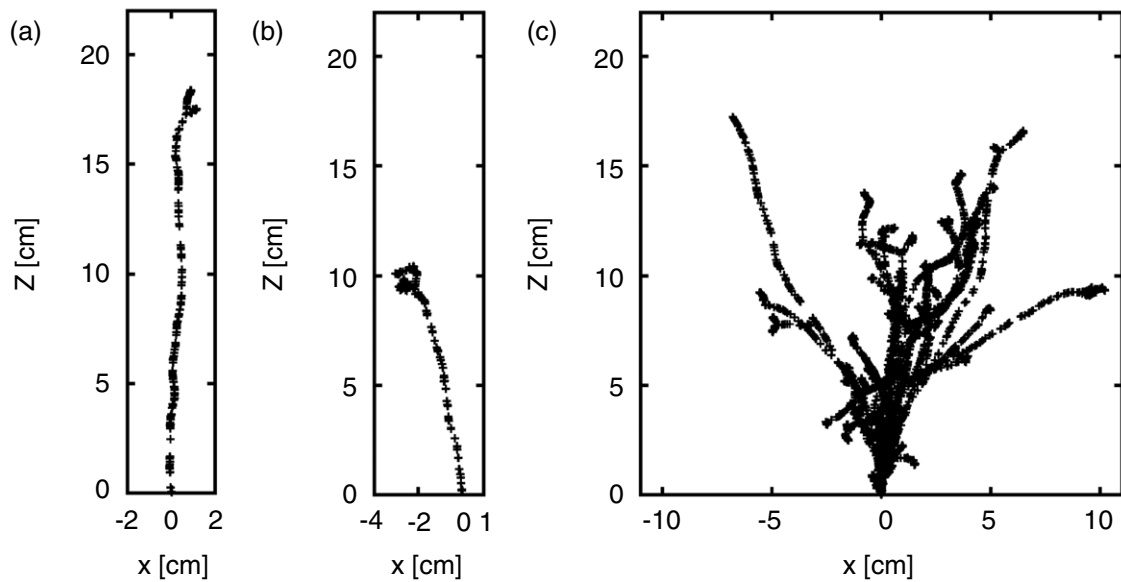


Figure 7. The spatial structure of an electron swarm for initial energy 1 MeV at 1 bar after approximately 0.8 ns (when the maximal electron number is reached): The position of electrons projected onto the xz plane for a swarm generated by (a) one initial electron, (b) one initial electron with a different realization of random numbers and (c) 20 initial electrons each with initial energy 1 MeV. All calculations are done without electrostatic interactions, i.e. (c) shows the superposition of 20 shower realizations as plotted in (a) and (b).

where $\epsilon_0 \approx 8.85 \times 10^{-12} \text{ A s V}^{-1} \text{ m}^{-1}$ and $N_e(t)$, $N_{i+}(t)$ and $N_{i-}(t)$ are the numbers of electrons, positive and negative ions at time t . The field strength ranges from approximately 10^{-5} V m^{-1} at 0.1 ns when the shower just starts to develop to approximately 10 V m^{-1} at 35 ns. Figure 9 explicitly shows the absolute value $|E|(r, t)$ in the xz plane after 35 ns when most electrons have already attached.

3.5. Energy of electrons and O^- ions

Figure 10 shows the electron energy spectrum after 1 ns for a shower in 1 bar air started by 100 electrons with an initial energy of $E_0 = 1 \text{ keV}$. There is a gap in the energy spectrum at approximately 0.1 eV; this is the energy range where three-body attachment dominates over other processes.

Figure 11 shows how the mean electron energy decreases in time in a 1 MeV shower and that the most energetic electrons are in the front part of the shower. The

energy of the electrons in the tail tends to approximately 1.0 eV. Thus most of them cannot ionize the background gas and the electron number does not increase further at these positions. After 0.8 ns the mean energy is almost independent of z and amounts to approximately 1.0 eV; this is the energy regime when attachment dominates over impact ionization.

Figure 12 shows this evolution on a logarithmic time scale, with the electron number and the mean energy of the complete electron shower as a function of time. It also shows explicitly that the electron number starts to decay when the average electron energy $\langle E_{\text{kin}} \rangle$ approaches 1 eV. As figure 10 shows, there is a gap in the energy regime of three-body attachment at 0.1 eV which is more significant at higher pressures. This is probably the reason why the mean energy saturates to a value of 1.0 eV for 1 bar and only to 0.9 eV for 100 mbar. Figure 13 shows that O^- ions are produced by electrons with kinetic energy of approximately 10 eV, actually independently of their

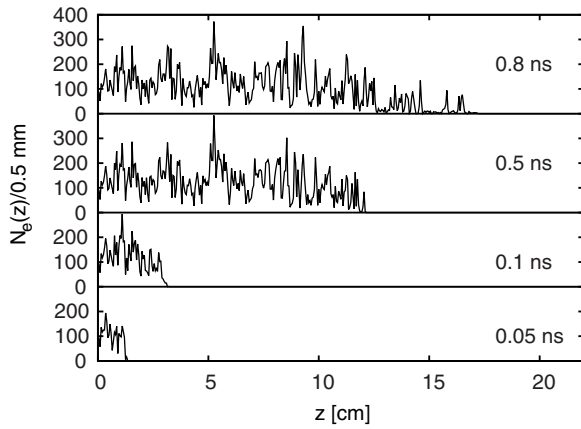


Figure 8. The electron number N_e as a function of z for bins of length $\Delta z = 0.5$ mm for $E_0 = 1$ MeV and 1 bar at $t = 0.05$ ns, $t = 0.1$ ns, $t = 0.5$ ns, $t = 0.8$ ns. We started the simulation with and averaged the electron number over 20 electrons.

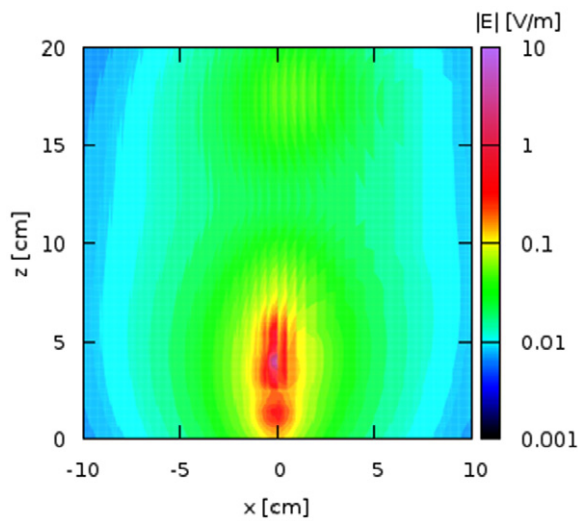


Figure 9. The electric field $|E|$ [V/m] induced by space charge effects at $t = 35$ ns in a swarm of one initial electron with $E_0 = 1$ MeV and 1 bar in the xz plane. This is a late stage of the shower plotted in figure 7(a).

initial energy E_0 . The kinetic energy of most O^- ions is below 1 eV. Thus detachment from O^- ions cannot play a significant role. Detachment from O^- would play a role in increasing the number of electrons at pressures below 10 mbar [34] where the number of O_2^- is negligible. Even so, an ambient electric field [34] would be needed.

4. Influence of an ambient electric field

Figure 14 shows the electron number and the mean energy of electrons in an external field at 1 bar. The initial energies of the incident electrons are $E_0 = 1$ keV and $E_0 = 1$ MeV. For 1 keV electrons and for electric fields of 5 or 8 kV cm⁻¹ the friction force through inelastic collisions with molecules is larger than the electric acceleration force [45]; thus all electrons eventually attach to oxygen. But for 1 MeV and 5 kV cm⁻¹ as well as 8 kV cm⁻¹ the electric force on average is larger than the friction force, and the shower grows and

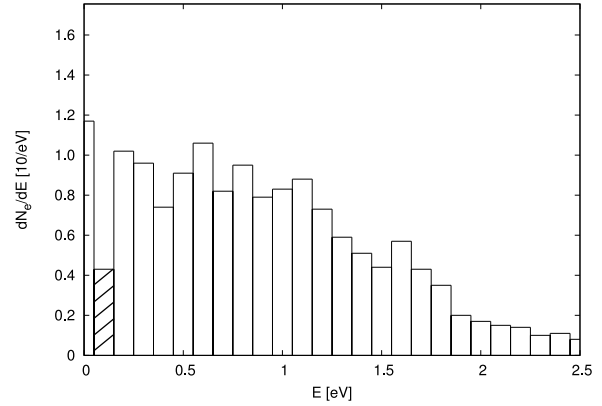


Figure 10. The electron energy spectrum at 1 ns in the low-energy range from 0 to 2.5 eV. The shower was generated by and averaged over 100 electrons in 1 bar air if $E_0 = 1$ keV. The hatched area indicates the gap where three-body attachment is dominant. The bin size is 0.1 eV.

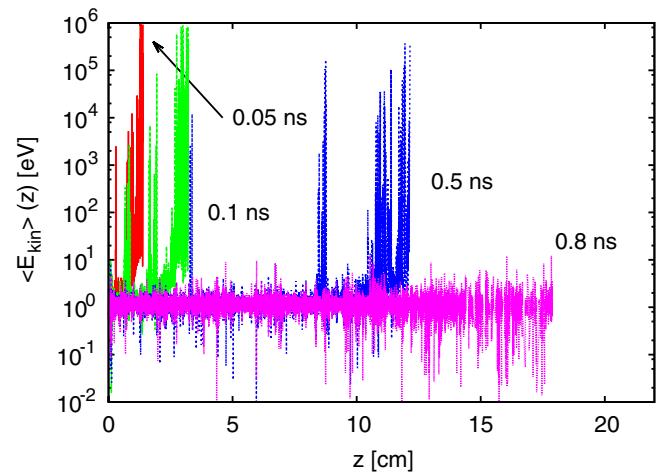
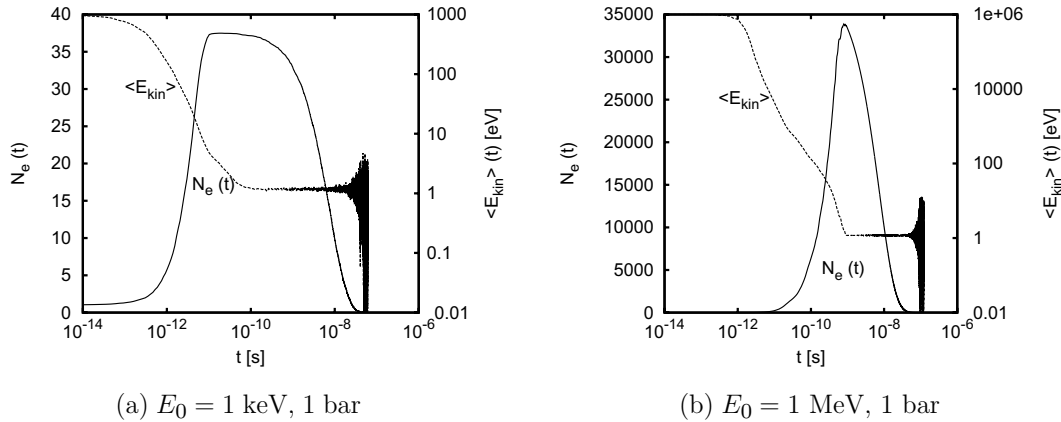


Figure 11. The average energy $\langle E_{kin} \rangle$ per bin $\Delta z = 0.01$ mm as a function of z for $E_0 = 1$ MeV and 1 bar at $t = 0.05$ ns (red), $t = 0.1$ ns (green), $t = 0.5$ ns (blue) and $t = 0.8$ ns (purple). We started the simulation with 20 electrons.

becomes a relativistic run-away electron avalanche (RREA). We note here that the breakdown field of classical breakdown is approximately 3 MV m⁻¹ [46] while the breakdown field for run-away breakdown is 0.3 MV m⁻¹ [47].

But even if no RREA is formed finally, the electrons gain more energy in a shower aligned with the electric field, and the number density and duration of the shower is higher than without electric field. A 1 keV electron creates 39 electrons in a field of 5 kV cm⁻¹ and 41 in a field of 8 kV cm⁻¹, rather than 37 without field. For 0 or 5 kV cm⁻¹, it takes approximately 1 ns till the electron number decreases. But for 8 kV/cm the plateau lasts for approximately 14 ns; thus it takes a factor of 14 longer. Since electrons gain energy from the external field, the mean electron energy $\langle E_{kin} \rangle$ in the shower is higher as well. It relaxes to approximately 1.6 eV for 5 kV cm⁻¹ or to 2.0 eV for 8 kV cm⁻¹. This is considerably higher than the 1.0 eV in vanishing field (see figure 12).

Figure 15 explicitly shows the low-energy spectrum of the electrons for 8 kV cm⁻¹ and for a 1 keV electron (the case of figure 14(b)). In contrast to figure 10 the electron


 (a) $E_0 = 1$ keV, 1 bar

 (b) $E_0 = 1$ MeV, 1 bar

Figure 12. The electron number and the mean electron energy as a function of time if the energy of the initial electron was (a) $E_0 = 1$ keV (100 initial electrons) and (b) $E_0 = 1$ MeV (20 initial electrons); the pressure is 1 bar in both cases. The mean energy fluctuations at the end appear because the electron number becomes small.

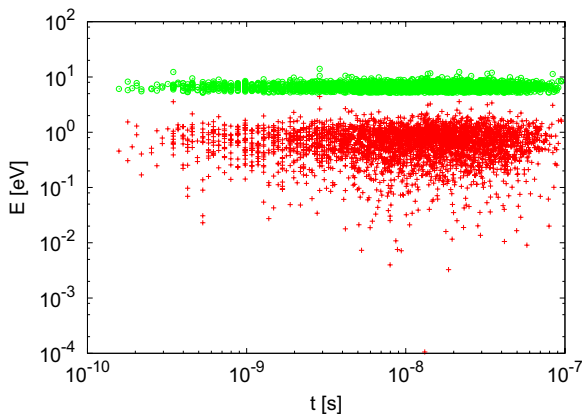


Figure 13. The energy of the electrons (green) attaching to oxygen and the energy of O^- (red) as a function of time for 1 bar and $E_0 = 1$ MeV. Every single point represents one electron attaching to oxygen or a O^- ion created by an electron, respectively.

number below 0.05 eV is negligible. Thus the gap of figure 10 is not visible in figure 15 although the electron number at 0.1 eV is similar. Without electric field the maximum of the spectrum lies at approximately 0.5 eV. At 8 kV cm^{-1} it lies at approximately 1 eV because of the energy gain by the ambient field. The average energy of 2 eV, however, is larger than 1 eV since there are still electrons in the energy tail up to 100 eV.

Since the number and energy of electrons is higher than in the case without ambient field, it takes longer till all electrons attach. Instead of 65 ns, it takes approximately 100 ns (for 5 kV cm^{-1}) and 500 ns (for 8 kV cm^{-1}) for all electrons to disappear. As stated in section 3.1, the exponential decay time without field is 8.19 ns. For 8 kV cm^{-1} it is approximately 80 ns which agrees well with data of [43] where they have simulated the motion of streamers in air in an ambient field of 10 kV cm^{-1} with a fluid model.

5. Conclusion and outlook

We have simulated the motion of electrons with initial energies $E_0 = 1$ keV, 10 keV, 100 keV and 1 MeV at 10 mbar, 100 mbar

and 1000 mbar with and without an ambient electric field and analyzed the spatial and energy distribution of the shower electrons as well as the swarm induced electric field in great detail.

We have seen that the electron number first increases due to ionization and then decreases because of the two-body and three-body attachment of electrons at oxygen. We have seen that the growth rate of the electron number is inversely proportional to the pressure, but that the decay is not. The average input energy per ion ranges from approximately 20 eV for 1 keV till 33 eV for 1 GeV; for 250 MeV we obtain an energy of approximately 33 eV/ion as given in [41]. We have shown that more subsequent ionizations of a secondary electron are more probable for small incident electron energies and thus the energy per ion pair decreases for decreasing initial electron energy.

The exponential decay time depends on the pressure and is about 10 ns for 1 bar as mentioned in [1, 43, 44] and $\approx 61 \mu\text{s}$ for 0.01 bar. The mean electron energy tends to 1 eV. The energy spectrum of electrons shows that there is a gap at ≈ 0.1 eV where three-body attachment is dominant. For 100 mbar and 1000 mbar the production of O_2^- ions through three-body attachment is dominant; for 10 mbar it is the production of O^- ions.

We have shown that the energy dissipates as a function of time and space. While the shower propagates, the mean energy saturates to 1 eV when the maximal electron number is reached. We have calculated the electric field created by electrons and residual ions. For 1 MeV we have shown that the field is at most 10 V m^{-1} in the vicinity of the origin of the shower. Thus space charge effects can be neglected for those energies.

We have also investigated the influence of two different ambient fields on the maximal electron number and the exponential decay time for initial electron energies of 1 keV and 1 MeV. For 1 keV and fields of 5 kV cm^{-1} and 8 kV cm^{-1} the friction force on average is larger than the electric force [45]. Thus there is no continuous growth of the electron number; however, the electron number and the exponential decay time are larger than without ambient field; for 8 kV cm^{-1}

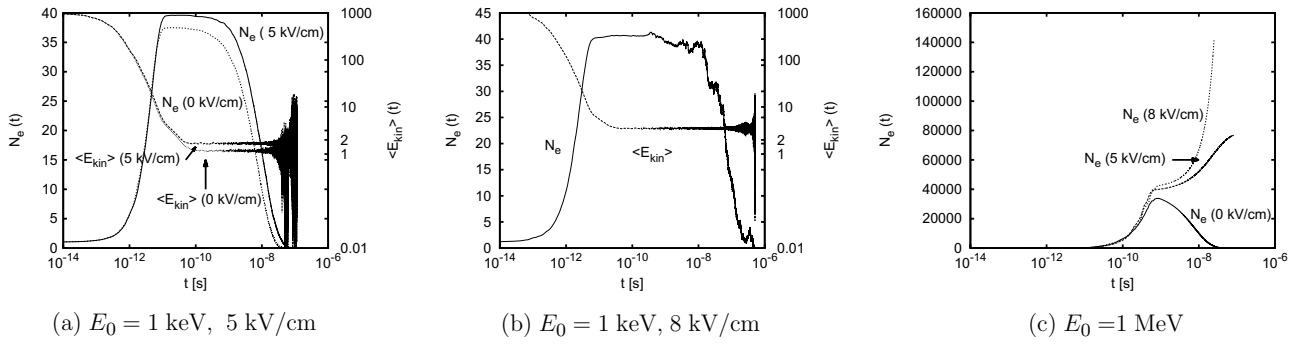


Figure 14. The electron number and the mean electron energy as a function of time for different external electric fields. The electric field amounts to (a) 5.0 kV cm^{-1} , (b) 8.0 kV cm^{-1} . The initial energy is $E_0 = 1 \text{ keV}$; the pressure is 1 bar. (a) also shows the electron number and mean energy without electric field. (c) The electron number for $E_0 = 1 \text{ MeV}$ at 1 bar as function of time without electric field and for 5 kV cm^{-1} as well as for 8 kV cm^{-1} .

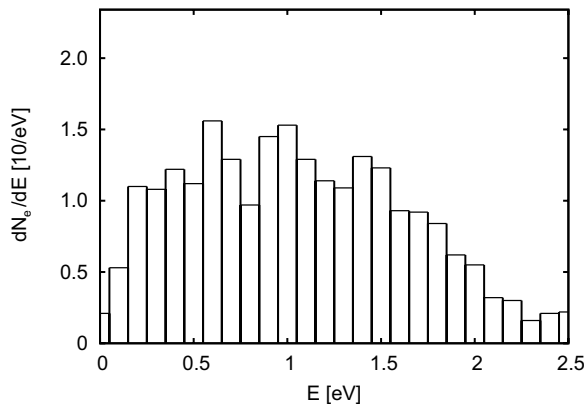


Figure 15. The energy spectrum in the low-energy range where attachment is dominant after 1 ns. The energy of the initial electron was $E_0 = 1 \text{ keV}$, and the ambient field 8 kV cm^{-1} , as in figure 14(b). The bin size is 0.1 eV.

the decay time is about 80 ns. For 1 MeV the friction force is smaller and thus an electron avalanche forms and the electron number continues increasing.

In the future high-energy particle models, i.e. for particles between 10^{20} eV and 1 MeV, and low-energy particle models (for energies $\leq 1 \text{ MeV}$) should be coupled. Beyond that, electric fields should be included. Thus the whole physics of a particle shower starting with particle energies of up to 10^{20} eV and propagating through an electric field can be captured. By coupling these two models, it will be possible to investigate the correlation between cosmic particle showers and the inception of lightning and vice versa the influence of thunderstorm fields on the detection of particle showers.

Acknowledgments

We would like to thank Olaf Scholten from the Kernfysisch Versneller Instituut (KVI), Groningen, The Netherlands, with whom we had fruitful discussions to improve this paper.

Furthermore, CK acknowledges financial support by STW-project 10757, where Stichting Technische Wetenschappen (STW) is part of The Netherlands' Organization for Scientific Research NWO.

Appendix A. The relativistic binary-encounter Bethe (RBEB) approach

In this appendix we will derive an explicit expression for Equation (4). The total cross section for ionization in the RBEB model is [25]

$$\sigma_{\text{RBEB}}(E_{\text{kin}}) = \frac{4\pi a_0^2 \alpha^4 N}{(\beta_t^2 + \beta_u^2 + \beta_b^2) 2b'} \times \left\{ \frac{1}{2} \left[\ln \left(\frac{\beta_t^2}{1 - \beta_t^2} \right) - \beta_t^2 - \ln(2b') \right] \left(1 - \frac{1}{t^2} \right) + 1 - \frac{1}{t} - \frac{\ln t}{t+1} \frac{1+2t'}{(1+t'/2)^2} + \frac{b'^2}{(1+t'/2)^2} \frac{t-1}{2} \right\}, \quad (\text{A.1})$$

where E_{kin} is the kinetic energy of the incident electron, $a_0 \approx 0.0529 \times 10^{-10} \text{ m}$ the Bohr radius, $\alpha \approx 1/137$ the fine structure constant and N the orbital electron occupation number, e.g. $N_{N_2} = 10$ and $N_{O_2} = 12$. The β_i are defined as

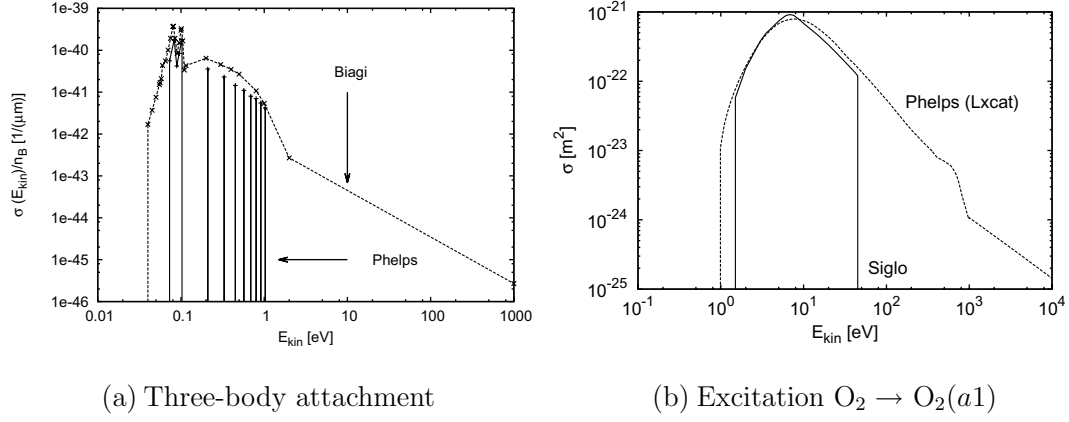
$$\beta_i^2 := 1 - \frac{1}{(1+i')^2}, \quad i \in \{t, b, u\} \quad (\text{A.2})$$

with $t := E_{\text{kin}}/B$ and

$$i' := \frac{I}{m_e c^2}, \quad I \in \{T = E_{\text{kin}}, B, U\}, \quad (\text{A.3})$$

where B is the ionization energy and U the kinetic energy of the bound electron on the shell, $m_e \approx 9.1 \times 10^{-31} \text{ kg}$ the electron mass and $c \approx 3 \times 10^8 \text{ m s}^{-1}$ the speed of light. The singly differential cross section is

$$\frac{d\sigma}{dW} = \frac{4\pi a_0^2 \alpha^4 N}{(\beta_t^2 + \beta_u^2 + \beta_b^2) 2b'} \times \left\{ \frac{\frac{N_i}{N} - 2}{t+1} \left(\frac{1}{w+1} + \frac{1}{t-w} \right) \frac{1+2t'}{(1+t'/2)^2} + \left(2 - \frac{N_i}{N} \right) \left[\frac{1}{(w+1)^2} + \frac{1}{(t-w)^2} + \frac{b'^2}{(1+t'/2)^2} \right] + \frac{1}{N(w+1)} \frac{df}{dw} \left[\ln \left(\frac{\beta_t^2}{1 - \beta_t^2} \right) - \beta_t^2 - \ln(2b') \right] \right\}, \quad (\text{A.4})$$



(a) Three-body attachment

 (b) Excitation $\text{O}_2 \rightarrow \text{O}_2(a1)$

Figure C1. (a) The total cross section for three-body attachment normalized to the gas density $2.6884 \times 10^{19} \text{ cm}^{-3}$ as a function of the energy E_{kin} of the incident electron by Phelps [33] and Biagi [49]. (b) Cross sections [22, 33, 50] for the electronic excitation $\text{O}_2 \rightarrow \text{O}_2(a1)$ as a function of incident electron energy E_{kin} .

where W is the kinetic energy of the emitted electron and $w := W/B$. df/dw is the differential dipole oscillator strength which determines N_i through

$$N_i := \int_0^\infty \frac{df}{dw} dw. \quad (\text{A.5})$$

The integrals in Equation (4) can be calculated analytically:

$$\begin{aligned} \int_{E_{min}}^A \frac{d\sigma}{d\bar{W}}(E_{kin}, \bar{W}) d\bar{W} &= \frac{4\pi a_0^2 \alpha^4 N}{(\beta_t^2 + \beta_u^2 + \beta_b^2) 2b'} \\ &\times \left\{ -\frac{1}{t+1} \frac{1+2t'}{(1+t'/2)^2} B \ln \left(\frac{(A/B+1)(t - E_{min}/B)}{(E_{min}/B+1)(t - A/B)} \right) \right. \\ &+ (A - E_{min}) \left(\frac{1}{(t - A/B)(t - E_{min}/B)} \right. \\ &+ \left. \frac{1}{(A/B+1)(E_{min}/B+1)} + \frac{b^2}{(1+t'/2)^2} \right) \\ &- \left. \frac{1}{2} B \left[\ln \left(\frac{\beta_t^2}{1-\beta_t^2} \right) - \beta_t^2 - \ln(2b') \right] \right\} \\ &\times \left[\frac{1}{(A/B+1)^2} - \frac{1}{(E_{min}/B+1)^2} \right] \end{aligned} \quad (\text{A.6})$$

with [25, 48]

$$\frac{df}{dw} := \frac{N_i}{(w+1)^2}. \quad (\text{A.7})$$

and

$$\frac{N_i}{N} \equiv 1 \quad (\text{A.8})$$

for the binary-encounter-Bethe (BEB) model.

Inserting $E_{kin}/2$ or W for A , Equation (4) becomes

$$\begin{aligned} R &= \left[-\frac{1}{t+1} B \ln \left(\frac{(W/B+1)(t - E_{min}/B)}{(E_{min}/B+1)(t - W/B)} \right) \frac{1+2t'}{(1+t'/2)^2} \right. \\ &+ \left. (W - E_{min}) \left(\frac{1}{(t - W/B)(t - E_{min}/B)} + \frac{1}{(W/B+1)(E_{min}/B+1)} \right) \right] \end{aligned}$$

$$\begin{aligned} &+ \frac{b^2}{(1+t'/2)^2} - \frac{1}{2} B \left[\ln \left(\frac{\beta_t^2}{1-\beta_t^2} \right) - \beta_t^2 - \ln(2b') \right] \\ &\times \left[\frac{1}{(W/B+1)^2} - \frac{1}{(E_{min}/B+1)^2} \right] \\ &\times \left[-\frac{1}{t+1} B \ln \left(\frac{(E_{kin}/2B+1)(t - E_{min}/B)}{(E_{min}/B+1)(t - E_{kin}/2B)} \right) \frac{1+2t'}{(1+t'/2)^2} \right. \\ &+ \left. \left(\frac{E_{kin}}{2} - E_{min} \right) \left(\frac{1}{(t - E_{kin}/2B)(t - E_{min}/B)} \right) \right. \\ &+ \left. \frac{1}{(E_{kin}/2B+1)(E_{min}/B+1)} + \frac{b^2}{(1+t'/2)^2} \right) \\ &- \left. \frac{1}{2} B \left[\ln \left(\frac{\beta_t^2}{1-\beta_t^2} \right) - \beta_t^2 - \ln(2b') \right] \right] \\ &\times \left[\frac{1}{(E_{kin}/2B+1)^2} - \frac{1}{(E_{min}/B+1)^2} \right]^{-1}. \end{aligned} \quad (\text{A.9})$$

Appendix B. Speed of oxygen ions

We will derive an expression in two steps for the speed of O and O^- produced through dissociative attachment. First we will show that $v_{\text{O}} = v_{\text{O}^-}$ and then we give expressions for v_{O} . To show that $v_{\text{O}} = v_{\text{O}^-}$, we start with the conservation of energy and momentum in the rest frame of oxygen, thus $v_{\text{O}_2} \equiv 0$:

$$\frac{m_e v^2}{2} = m_{\text{O}} \frac{v_{\text{O}}^2}{2} + m_{\text{O}} \frac{v_{\text{O}^-}^2}{2} + E_{\text{bind}} \quad (\text{B.1})$$

$$m_e v = m_{\text{O}} v_{\text{O}} + m_{\text{O}} v_{\text{O}^-} \quad (\text{B.2})$$

where we used non-relativistic expressions for energy and momentum because of the small velocity of all particles. Since the electron mass is much smaller than the mass of O and O^- and we are in the non-relativistic regime, we can approximate $m_e v \approx 0$, thus

$$0 = m_{\text{O}} v_{\text{O}} + m_{\text{O}} v_{\text{O}^-} \Rightarrow v_{\text{O}} = -v_{\text{O}^-}. \quad (\text{B.3})$$

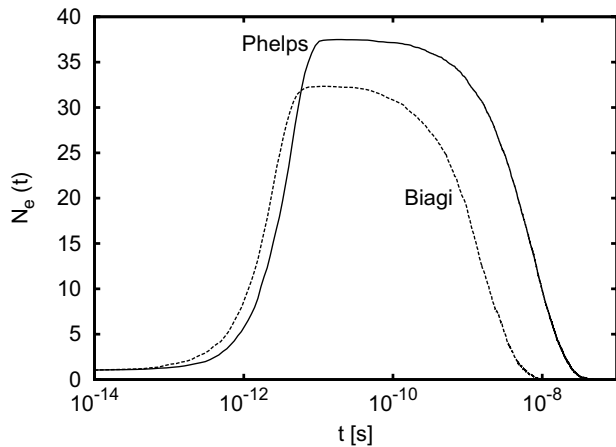


Figure C2. The electron number \bar{N}_e as a function of time in the case of $E_0 = 1$ keV using the cross sections of Phelps and Biagi for electronic excitations and attachment [33, 49].

Using Equation (B.3), (B.1) leads to

$$v_0 = v_{0^-} = \sqrt{\frac{m_e |v|^2}{2m_0} - \frac{E_{\text{bind}}}{m_0}} \quad (\text{B.4})$$

where v is the velocity of the electron.

Appendix C. Dependence on the cross sections

The results depend sensitively on the cross sections as input data. Figure C1(a) shows the cross sections for three-body attachment by Phelps [33] and Biagi [49] normalized to gas density. It shows that these two cross sections have different lower and upper threshold energies. Figure C1(b) shows the cross sections for electronic excitation $\text{O}_2 \rightarrow \text{O}_2(a1)$ from the SIGLO database [50] and the LXcat database [22], Phelps [33]. Figure C2 compares the time evolution of the electron number if $E_0 = 1$ keV. Using data for excitation of [50] and attachment of [49], the maximal electron number is 32 and the attachment time is approximately 1 ns. However, using data for excitation of [22] and attachment of [33] yields to a maximum of 37 electrons, the exponential decay time is approximately 8 ns. Thus we can conclude that the time evolution is different for different kind of cross sections and that the data of [50] and Biagi [49] lead to an unphysically short attachment time.

References

- [1] Nijdam S *et al* 2011 Probing background ionization: positive streamers with varying pulse repetition rate and with a radioactive admixture *J. Phys. D: Appl. Phys.* **44** 455201
- [2] Gurevich A V *et al* 2007 Runaway breakdown in strong electric field as a source of terrestrial gamma flashes and gamma bursts in lightning leader steps *Phys. Lett. A* **361** 119–25
- [3] Celestin S and Pasko V P 2011 Energy and fluxes of thermal runaway electrons produced by exponential growth of streamers during the stepping of lightning leaders and in transient luminous events *J. Geophys. Res.* **116** A03315
- [4] Kutsyk I M *et al* 2011 Self-sustained relativistic runaway electron avalanches in the transverse field of lightning leader as sources of terrestrial gamma-ray flashes *JETP Lett.* **94** 606–9
- [5] Xu W *et al* 2012 Source altitudes of terrestrial gamma-ray flashes produced by lightning leaders *Geophys. Res. Lett.* **39** L08801
- [6] Kochkin P O *et al* 2012 Experimental study of hard x-rays emitted from metre-scale positive discharges in air *J. Phys. D: Appl. Phys.* **45** 425202
- [7] Kochkin P O *et al* 2014 Experimental study of the spatio-temporal development of meter-scale negative discharge in air *J. Phys. D: Appl. Phys.* **47** 145203
- [8] Linsley J 1963 Evidence for a primary cosmic-ray particle with energy 10^{20} eV *Phys. Rev. Lett.* **10** 146–8
- [9] Chakraborti S *et al* 2011 Ultra-high-energy cosmic ray acceleration in engine-driven relativistic supernovae *Nature Commun.* **2** 175
- [10] Dermer C D *et al* 2009 Ultra-high-energy cosmic rays from black hole jets of radio galaxies *New J. Phys.* **11** 065016
- [11] Bhattacharjee P and Sigl G 2000 Origin and propagation of extremely high-energy cosmic rays *Phys. Rep.* **327** 109–247
- [12] Siingh D and Singh R P 2010 The role of cosmic rays in the Earth's atmospheric processes *Pramana J. Phys.* **71** 153–68
- [13] Babich L P *et al* 2011 Lightning initiation mechanism based on the development of relativistic runaway electron avalanches triggered by background cosmic radiation: numerical simulation *J. Exp. Theor. Phys.* **112** 902–9
- [14] Brown W C *et al* 2012 A beginning investigation into the possible role of cosmic rays in the initiation of lightning discharges at the Pierre Auger Observatory *Eur. Phys. J. Plus* **127** 95
- [15] Gurevich A V *et al* 2004 New type discharge generated in thunderclouds by joint action of runaway breakdown and extensive atmospheric shower *Phys. Lett. A* **329** 348–61
- [16] Carlson B E *et al* 2008 Runaway relativistic electron avalanche seeding in the Earth's atmosphere *J. Geophys. Res.* **113** A10307
- [17] Babich L P *et al* 2012 Numerical simulations of local thundercloud field enhancement caused by runaway avalanches seeded by cosmic rays and their role in lightning initiation *J. Geophys. Res. Space Phys.* **117** A09316
- [18] www-ik.fzk.de/~corsika/
- [19] Capdevielle J N *et al* 2000 Simulation of extensive air showers at ultra-high energy using the CORSIKA Monte Carlo code *Astropart. Phys.* **13** 259–75
- [20] Knapp J *et al* 2003 Extensive air shower simulations at the highest energies *Astropart. Phys.* **19** 77–99
- [21] Cherenkov P A 1934 Visible emissions of clean liquids by action of γ radiation *Dokl. Akad. Nauk SSSR* **2** 451
- [22] Electron scattering database, www.lxcat.laplace.univ-tlse.fr
- [23] Li C *et al* 2012 Spatially hybrid computations for streamer discharges: II. Fully 3D simulations *J. Comput. Phys.* **231** 1020–50
- [24] Li C *et al* 2009 3D hybrid computations for streamer discharges and production of runaway electrons *J. Phys. D: Appl. Phys.* **42** 202003
- [25] Kim Y-K and Santos J P and Parente F 2000 Extension of the binary-encounter-dipole model to relativistic incident electrons *Phys. Rev. A* **62** 052710
- [26] Jacob J H 1973 Multiple electron-scattering through a slab *Phys. Rev. A* **8** 226–35
- [27] Phelps A V and Pitchford L C 1985 Anisotropic scattering of electrons by N_2 and its effect on electron transport *Phys. Rev. A* **31** 2932–49
- [28] Phelps A V 1985 *JILA Information Center Report No 28*, University of Colorado
- [29] Fiala A *et al* 1994 2-dimensional, hybrid model of low-pressure glow-discharges *Phys. Rev. E* **49** 5607–22

- [30] Vahedi V and Surendra M 1995 A Monte Carlo collision model for the particle-in-cell method applications to argon and oxygen discharges *Comput. Phys. Commun.* **87** 179–98
- [31] Bethe H A and Heitler W 1934 On the stopping of fast particles and on the creation of positive electrons *Proc. Phys. Soc. Lond.* **146** 83–112
- [32] Koehn C and Ebert U 2014 Angular distribution of Bremsstrahlung photons and of positron beams *Atmos. Res.* **135–136** 432–65
- [33] Lawton S A and Phelps A V 1978 Excitation of $b^1\Sigma_g^+$ state of O_2 by low-energy electrons *J. Chem. Phys.* **69** 1055–68
- [34] Luque A and Gordillo-Vázquez F J 2012 Mesospheric electric breakdown and delayed sprite ignition caused by electron detachment *Nature Geosci.* **5** 22–5
- [35] Murphy T 1988 Total and differential electron collision cross sections for O_2 and N_2 *Report LA-11288-MS* Los Alamos National Laboratory
- [36] Shyn T W *et al* 1972 Angular distribution of electrons elastically scattered from N_2 *Phys. Rev. A* **6** 1002–12
- [37] Celestin S and Pasko V P 2010 Soft collisions in relativistic runaway electron avalanches *J. Phys. D: Appl. Phys.* **43** 315206
- [38] Burden R L and Faires J D 2000 *Numerical Analysis* (Scarborough, Canada: Brookes/Cole) ISBN 0-534-38216-9
- [39] Gordillo F J 2008 Air plasma kinetics under the influence of sprites *J. Phys. D: Appl. Phys.* **41** 234016
- [40] Peralta L 2002 Monte Carlo simulation of neutron thermalization in matter *Eur. J. Phys.* **23** 307–14
- [41] Suwada T, Ohsawa S, Furukawa K and Akasaka N 2000 Absolute beam-charge measurements for single-bunch electron beams *Japan. J. Appl. Phys.* **39** 628–34
- [42] Arqueros F, Blanco F and Rosado J 2009 Analysis of the fluorescence emission from atmospheric nitrogen by electron excitation, and its application to fluorescence telescopes *New J. Phys.* **11** 065011
- [43] Morrow R and Lowke J J 1997 Streamer propagation in air *J. Phys. D: Appl. Phys.* **30** 614–27
- [44] Pancheshnyi S 2005 Role of electronegative gas admixture in streamer start, propagation and branching phenomena *Plasma Sources Sci. Technol.* **14** 645–53
- [45] Gurevich A V 1961 On the theory of runaway electrons *Sov. Phys.—JETP* **12** 904–12
- [46] Milikh G M and Roussel-Dupré R 2010 Runaway breakdown and electrical discharges in thunderstorms *J. Geophys. Res.* **115** A00E60
- [47] Gurevich A V, Milikh G M and Roussel-Dupré R 1992 Runaway electron mechanism of air breakdown and preconditioning during a thunderstorm *Phys. Lett. A* **165** 463–8
- [48] Kim Y K and Rudd M E 1994 Binary-encounter-dipole model for electron-impact ionization *Phys. Rev. A* **50** 3954–67
- [49] 2012 Transcribed from S F Biagi's FORTRAN code Magboltz, version 8.97 <http://consult.cern.ch/writeup/magboltz/>
- [50] The Siglo Database, CPAT and Kinema Software, www.siglo-kinema.com